ACS Sustainable Chemistry & Engineering

Research Article

pubs.acs.org/journal/ascecg

Green One-Step Synthesis of Catalytically Active Palladium Nanoparticles Supported on Cellulose Nanocrystals

Marzieh Rezayat,[†,#] Rebecca K. Blundell,[‡] Jason E. Camp,[‡,§] Darren A. Walsh,[‡] and Wim Thielemans*[,‡,∥,⊥]

[†]Department of Chemistry, Isfahan University of Technology, Isfahan 84156-83111, Islamic Republic of Iran

[‡]School of Chemistry, The University of Nottingham, University Park, Nottingham NG7 2RD, United Kingdom

[§]School of Biological and Chemical Sciences, Queen Mary University of London, London E1 4NS, United Kingdom

[∥]Process and Environmental Research Division, Faculty of Engineering, The University of Nottingham, Nottingham NG7 2RD, United Kingdom

Supporting Information

ABSTRACT: Palladium nanoparticles (PdNPs) supported on cellulose nanocrystals (CNXL) were synthesized in a single step from Pd(hexafluoroacetylacetonate)$_2$ (Pd(hfac)$_2$) in subcritical and supercritical carbon dioxide. CNXLs acted as both the reducing agent and support material for the obtained nanoparticles. Dry Pd nanoparticles supported on the cellulose nanocrystals (PdNP@CNXL) were obtained by simply venting the CO_2 and were characterized by FT-IR, X-ray photoelectron spectroscopy (XPS), powder X-ray diffraction (XRD), thermogravimetric analysis (TGA), and transmission electron microscopy (TEM). The results show that the Pd nanoparticle diameters varied between 6 and 13 nm with varying pressure (240−2200 psi), reaction time (2−17 h), and weight ratio of the precursor Pd(hfac)$_2$ to CNXL (1−4% w/w). Particles with diameters above 13 nm appeared not to remain attached to the CNXL surface. Reaction conditions also affected the Pd loading in the final PdNP@CNXL composite. Finally, the PdNP@CNXL composites were shown to be effective catalysts for carbon−carbon bond formation in the Mizoroki−Heck cross-coupling reaction, in line with other reports.

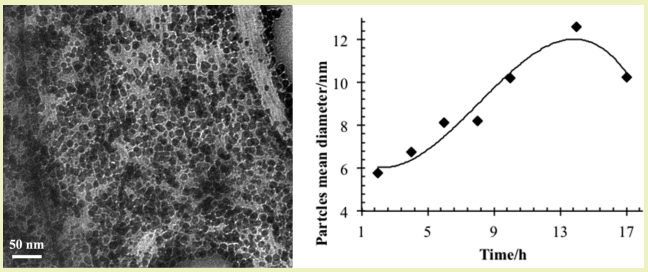

KEYWORDS: *Cellulose nanocrystals, Metal nanoparticles, Supercritical CO_2, Palladium catalysis, Polysaccharides, Green chemistry*

INTRODUCTION

The properties of nanoparticles are different from those of bulk materials due to their small size and large surface to volume ratio.[1] Among nanoparticles, transition metal nanoparticles have received a large amount of attention as catalysts for a wide range of chemical reactions.[2−6] In particular, palladium (Pd) is the most broadly used catalyst for the synthesis of fine chemicals in preparative chemistry and on an industrial scale[7] as both a heterogeneous and homogeneous catalyst.[8] Support of Pd on natural substrates has gained a lot of interest and has recently been reviewed.[9] However, in the form of nanoparticles, aggregation of naked Pd(0) nanoparticles (Pd black) is a very common problem due to the high reactivity and high surface/core atomic ratio.[10] As a result, catalyst activity and selectivity decreases with increased aggregation. The use of capping agents can reduce or prevent aggregation, but such agents tend to reduce the reactivity of the surface, thereby reducing the catalytic activity of the stabilized nanoparticles. An alternative approach is to support nanoparticles onto materials, which can reduce or prevent aggregation, without blocking access to the reactive surface atoms.[11] Supported palladium nanoparticles have recently been studied as catalysts for a range of reactions such as the catalytic hydrogenolysis of C−OH bonds,[12] catalytic hydrogenation,[13] Suzuki−Miyaura and Mizoroki−Heck cross-coupling reactions,[14] decolorization of azo dyes used in the treatment of wastewater,[15] and the selective hydrogenation of C═C bonds.[16] In addition, Lunsford et al. reported the use of supported Pd nanoparticles in catalyzing the direct formation of hydrogen peroxide from H_2 and O_2 for the first time.[17] Owing to the good electrocatalytic activity of Pd nanoparticles, they have also been used as the anode catalyst in direct formic acid fuel cells (DFAFCs)[18] and biosensors.[19]

The common synthetic methods for the preparation of metal nanoparticles are thermal decomposition or chemical reduction. To maximize the sustainability of nanoparticle production, their synthesis should make use of (i) a renewable or easily recyclable reducing agent, (ii) a renewable material for the stabilization of the nanoparticles, and (iii) an environmentally benign reaction medium.[20−22] Minimization of energy consumption and ease of nanoparticle recovery after synthesis should also be taken into account.

Received: February 7, 2014
Revised: March 23, 2014
Published: April 1, 2014

Several renewable materials have already been reported to act as both reducing agent and/or stabilizer. For example, β-D-glucose and starch have been used as the reducing agents and template for the synthesis of supported silver, gold, and palladium nanoparticles,[15,23,24] and cellulose or cellulose derivatives as both reducing agent and stabilizer for the synthesis of palladium, nickel, silver, gold, platinum, and selenium nanoparticles have also been reported.[25−31] Pd(0) nanoparticles supported on cellulose have generally been prepared with the use of an exogenous reducing agent,[32,33] though a "reagentless" method that was conducted under aqueous conditions was recently disclosed.[34] Use of a "reagentless" method and an easily removable solvent, such as a gas, would make the preparation of dry ready-to-use catalyst powder straightforward. It would reduce shipping costs, and any desired quantity could be added to a reaction system without the need for drying, concentrating, or separation.

Our research group has previously reported the inherent potential of cellulose nanocrystals (CNXLs) as a stable surface for reduction of metal ions and immobilization of metal nanoparticles due to its abundant surface hydroxyl groups; the syntheses of platinum and silver nanoparticles from their aqueous solution mixed with CNXL were performed in a $scCO_2$/water[35] and in a hydrothermal[36] system. Pt nanoparticles supported on carbon have also been prepared by CNXL reduction in water in the presence of mesoporous carbon to form electrocatalysts.[37] Furthermore, CNXLs have also been used as support material for catalytically active gold nanoparticles using $NaBH_6$ as the reducing agent for the formation of the gold nanoparticles,[38] while Cirtiu et al. reported CNXL-supported Pd nanoparticles using H_2 as the reducing agent and showed catalytic activity of the formed nanoparticles for catalytic hydrogenation and Heck coupling reactions.[13]

In this work, we set out to produce CNXL-supported Pd nanoparticles (PdNP@CNXL) through CNXL-induced reduction of Pd precursors in subcritical and supercritical carbon dioxide ($scCO_2$).This would have the dual benefits of not needing an exogenous reductant or immobilizing system and easy recovery of the supported catalyst by simply venting of CO_2. $ScCO_2$ has received a large amount of attention as an attractive environmentally benign solvent for chemical synthesis.[39−41] Some of the most important characteristics of $scCO_2$ are the modest conditions to reach the critical point (T_c = 31.0 °C, p_c = 73.9 bar/1072 psi), nonflammability, nontoxicity, inertness, and natural abundance. Furthermore, the $scCO_2$ solvent power is tunable by simply changing pressure and temperature,[42,43] while increased solubility can be obtained using the addition of fluorocarbons. The preparation of metallic nanoparticles in $scCO_2$ is an obvious extension of the properties of $scCO_2$, the availability of $scCO_2$ soluble organometallic complexes, and the ability to simply vent CO_2 after the reduction reaction to yield the reaction products, i.e., PdNP@CNXL.[44]

PdNP@CNXL composites were produced in subcritical and supercritical carbon dioxide as a benign solvent and $Pd(hfac)_2$ as the Pd precursor as it is soluble in both liquid and supercritical CO_2 at different pressures and temperatures.[45] The reducing ability of the CNXL surface hydroxyl groups was used to reduce the Pd precursor, removing the need to add an additional reducing agent, and resulting in CNXL-supported Pd nanoparticles (PdNP@CNXL) upon venting of the CO_2. The effect of pressure, reaction time, temperature, and ratio of the precursor $Pd(hfac)_2$ to CNXL were investigated, and the PdNP@CNXL composites were characterized with FT-IR, X-ray photoelectron spectroscopy (XPS), powder X-ray diffraction (XRD), transmission electron microscopy (TEM), and thermogravimetric analysis (TGA) in order to show how conditions affected formation of PdNP@CNXLs. As far as we know, a detailed study of the effect on preparation conditions on PdNPs on cellulose substrates has not yet been performed. The ability of the supported Pd nanoparticles to catalyze carbon−carbon bond formation was subsequently tested using two different Mizoroki−Heck reactions to show that the PDNPs formed under CNXL reduction in $scCO_2$ display the same activity as those prepared using exogenous reductants.

EXPERIMENTAL SECTION

Materials. Palladium(II) hexafluoroacetylacetonate, $Pd(hfac)_2$, acetone, and Amberlite MB 6113 were purchased from Sigma Aldrich and used as received. Cellulose nanocrystals were prepared from cotton as described before.[46] In brief, CNXLs were extracted from cotton wool via acid hydrolysis using a 64 wt % aqueous sulfuric acid solution for 35 min at 45 °C. The suspension was centrifuged, washed, and dialyzed with tap water to remove residual-free acid. A stable dispersion was obtained by sonication and filtration over a N°2 fritted filter to remove aggregates. Ion exchange resin Amberlite MB 6113 was then added to the dispersion under agitation for 1 h to protonate the CNXL surface and remove nonproton ions. Filtration was then used to remove the ion-exchange resin, and sonication was used to individualize the CNXLs. This stable dispersion was subsequently quickly frozen by immersion into liquid nitrogen, freeze-dried, and stored in a sealed glass container.

PdNP@CNXL Synthesis. [**Safety note**: Experiments with $scCO_2$ involve high pressures and should only be carried out in equipment with the appropriate pressure rating and safety operating procedures. Operators should also be trained to work safely with high pressure equipment.] The reaction vessel was a home-built 60 mL stainless steel high-pressure batch autoclave equipped with a mechanical stirrer and a heating sleeve surrounding the autoclave. The internal pressure was measured directly using a pressure sensor, which was also connected to the heating control.

In a typical run, specified amounts of CNXL and $Pd(hfac)_2$ were added to the autoclave. After the autoclave was sealed, it was flushed with CO_2 for several minutes. After flushing, CO_2 was introduced with a Pickel pump (NWA Analytics) while the heating jacket heated the autoclave. The pressure and temperature were increased simultaneously through all experiments. The mixture was subsequently stirred for the specified time, and the system was depressurized by placing the autoclave in a dry ice−acetone bath. Venting of the autoclave led to the reaction product. The sample was then washed with acetone for several times to remove unreacted precursor and unwanted byproduct (hexafluoroacetylacetone). During washing, the liquid phase was separated from the solid phase (PdNP@CNXL) by centrifugation. The cleaned sample was subsequently dried at 50 °C in a convection oven and finally stored in a closed glass vial under ambient conditions in air for characterization. The pressure in the autoclave was varied between 220 and 2240 psi, spanning subcritical and supercritical conditions while the reaction time ranged from 2 to 17 h.

Over the course of several months of performing the reduction reaction in the stainless steel vessel, no degradation of the reactor walls was noticed, which could have occurred under highly acidic conditions. Furthermore, no reduction of Pd was noticed without addition of CNXLs, showing that CNXLs were indeed instrumental in the reduction process.

It also has to be mentioned that the obtained PDNP@CNXLs could be readily dispersed in water by sonication. This is potentially very useful as good dispersibility is key to a high catalytic activity.

Characterization Techniques. *Powder X-ray Diffraction (XRD).* XRD data were collected on a PANalytical X'Pert Pro MPD X-ray diffractometer in Bragg−Brentano geometry using Cu$K\alpha_1$ (λ =

1.54056 A°) radiation operating at 40 kV and 40 mA with automated divergence and receiving slits (10 mm illuminated length), 10 mm beam mask, 0.04 rad soller slits, and a step size of 0.2°. X'Pert HighScore Plus analytical software was used to analyze the results.

X-ray Photoelectron Spectroscopy. XPS analysis was performed on dried solid samples from the reactor after purification and drying using a Kratos AXIS ULTRA spectrometer with a monochromated Al Kα X-ray source (hν = 1486.6 eV) and a delay line detector (DLD) with a takeoff angle of 90° and an acceptance angle of 30° while using charge neutralization. The X-ray gun power was set to 150 W. The spectra were recorded using an aperture slot of 300 μm × 700 μm with a pass energy of 80 eV for survey scans and 10 eV for high-resolution scans. All spectra were recorded using Kratos VISION II software and processed using CASAXPS software. The binding energy positions were referenced versus the C_{1s} at 285 eV. Pd(0) shows up as a doublet at 335.2 eV ($3d_{5/2}$) and 340.1 eV ($3d_{3/2}$), with Pd(II) signals at 337.3 eV ($3d_{5/2}$) and 341.5 eV($3d_{3/2}$). For all samples, the Pd(0) 3p3/2 signal was found not to interfere with O1s due to the relatively low Pd atom fraction (<5 at%), in agreement with other work.[47] Representative spectra can be found in the Supporting Information.

Fourier Transform Infrared (FT-IR). The FT-IR samples were prepared by forming a thin pellet of KBr and the Pd nanoparticles supported on CNXLs (98:2 weight ratio). A pure KBr pellet was used as background and was subtracted from the FT-IR spectra of the samples.

Thermogravimetric Analysis. The amount of Pd supported on CNXL was determined by thermogravimetric analysis using a Q500TGA through comparison of the thermal behavior of dried purified solid from the reactor with pure CNXL. For a typical test, about 5 mg of sample was heated from ambient temperature to 700 °C at a rate of 10 °C/min under air.

Transmission Electron Microscopy. TEM was performed on a JEOL 200FX operating at 100 kV. A dilute sample dispersion was deposited on a carbon coated copper grid and left for 3 min after which excess liquid was removed. The carbon-coated copper grid had been exposed to a 25:75 oxygen:argon atmosphere for 3 s prior to sample deposition to render it more hydrophilic.

Catalytic Application. The catalytic activity of PdNP@CNXL was tested using the Mizoroki−Heck, the addition of an aryl halide to an alkene, using the following experimental conditions to prepare methyl *trans*-cinnamate (Scheme 1) and (*E*)-stilbene (Scheme 2):

*Methyl trans-Cinnamate (**2**).* To a stirred suspension of PdNP@CNXL (4 mg, 35.2 wt % palladium, 0.013 mmol) in dry DMF (5 mL) at rt were added iodobenzene (0.11 mL, 1.0 mmol), methyl acrylate (0.11 mL, 1.2 mmol), and triethylamine (0.19 mL, 1.4 mmol). The resultant mixture was stirred for 16 h at 130 °C. The solvent was removed under reduced pressure, and the mixture was purified by flash column chromatography on silica gel (9:1 petroleum/EtOAc) to afford methyl *trans*-cinnamate (**2**) as a white crystalline solid (155 mg, 96%), which had spectra identical to that reported in the literature.[48] Mp: 36−37 °C. IR (CH_3Cl) ν_{max}: 3011, 2953, 1712, 1638, 1602, 1496, 1329, 1316, 1282, 1174, 980, 865 cm^{-1}. ^1H NMR (270 MHz, $CDCl_3$): δ 7.70 (d, J = 15.9 Hz, 1H), 7.55−7.45 (m, 2H), 7.40−7.37 (m, 3H), 6.45 (d, J = 15.9 Hz, 1H), 3.81 (s, 3H). ^{13}C NMR (68 MHz, $CDCl_3$): δ 167.5, 145.0, 134.5, 130.4, 129.0, 128.2, 117.9, 51.8. HRMS (EI^+) m/z: calcd for $C_{10}H_{10}NaO_2$ $(M + H)^+$ 185.0579; found, 185.0578.

*(E)-Stilbene (**3**).* To a stirred suspension of PdNP@CNXL (9.8 mg, 23.4 wt % palladium, 0.023 mmol) in acetonitrile/water (1:3, 1.15 mL) at rt were added sodium acetate (26 mg, 0.32 mmol), iodobenzene (0.03 mL, 0.27 mmol), and styrene (0.03 mL, 0.28 mmol). The resultant mixture was stirred for 16 h at 100 °C. CH_2Cl_2 (20 mL) and H_2O (20 mL) were added. The organic layer was dried over Na_2SO_4, and the solvent was removed under reduced pressure. The mixture was purified by flash column chromatography on silica gel (petroleum) to afford (*E*)-stilbene (**3**) as a white crystalline solid (42 mg, 87%), which had spectra identical to that reported in the literature.[49] Mp: 124−125 °C;.IR ($CHCl_3$) ν_{max}: 3081, 3062, 3010, 1600, 1497, 1453 1072, 1030, 984, 960 cm^{-1}. ^1H NMR (270 MHz, $CDCl_3$): δ 7.56−7.38 (m, 10H), 7.16 (s, 2H). ^{13}C NMR (68 MHz, $CDCl_3$): δ 137.4, 128.8, 128.3, 127.7, 126.6. HRMS (EI^+) m/z: calcd for $C_{14}H_{12}$ $(M + H)^+$ 180.0939; found, 180.0936.

Scheme 1. Methyl *trans*-Cinnamate Preparation Reaction Scheme

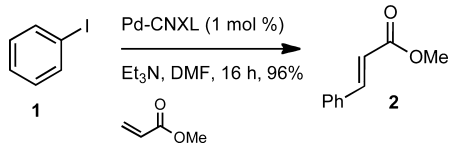

Scheme 2. (*E*)-Stilbene Preparation Reaction Scheme

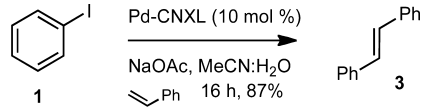

RESULTS AND DISCUSSION

The effects of pressure, reaction time, and $Pd(hfac)_2$ to the CNXL ratio on the Pd reduction and formation of PdNP@CNXLs were investigated independently, and the effects of each of these parameters are described below. Figure 1 shows a typical XRD pattern for cellulose nanowhisker-supported Pd nanoparticles from a typical experiment. Five peaks labeled around 40°, 46°, 68°, 82°, and 86° correspond to the crystal planes of Pd(0). The Scherrer equation was applied to the (111) peak of Pd to calculate the mean diameter of the synthesized Pd nanoparticles. The peak observed at 22.7° is the CNXL (200) crystal plane of the cellulose I_β polymorph.[46,50] Other cellulose peaks are of too low intensity to be seen in the diffractogram.

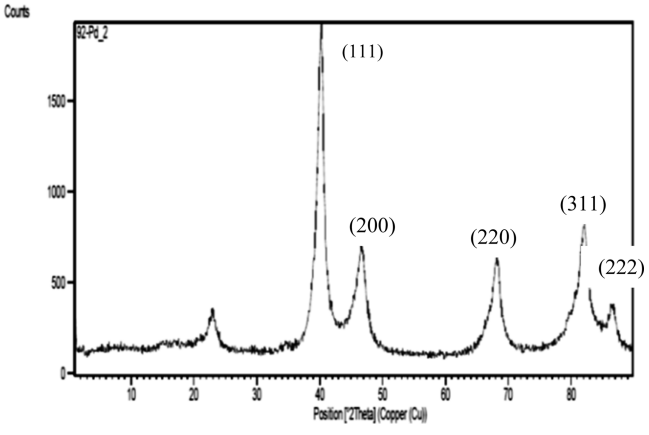

Figure 1. XRD pattern of a synthesized PdNPs supported on cellulose nanowhiskers in supercritical carbon dioxide at 100 °C, 1240 psi, and 17 h.

Effect of Pressure. Pd nanoparticles supported on CNXL were synthesized using subcritical and supercritical carbon dioxide by varying the pressure between 240 and 2200 psi (going through the supercritical point). The temperature, reaction time, and weight ratio of the precursor ($Pd(hfac)_2$) to CNXL were fixed at 100 °C, 17 h, and 2% w/w, respectively. For all pressures, the color of CNXL changed from white to dark gray or black due to loading of PdNPs onto the surface of CNXL. The X-ray diffractograms confirmed the formation of Pd nanoparticles by the appearance of Pd crystal plane signals

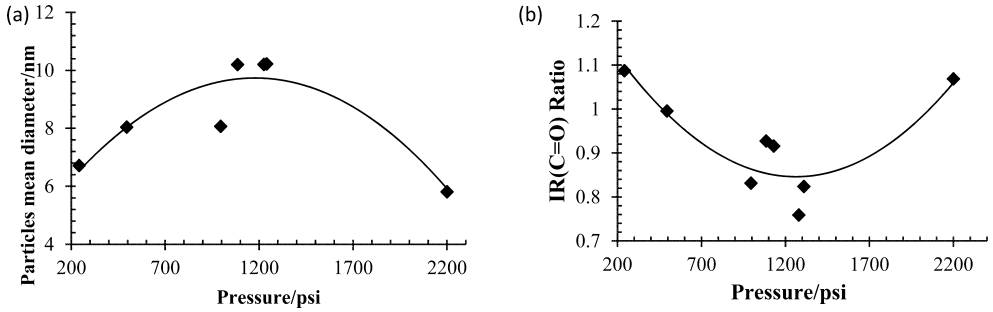

Figure 2. Effect of pressure on (a) the mean diameter of synthesized PdNP@CNXL and (b) the relative intensity of the FTIR signals from 1710 to 1630 cm^{-1} for the PdNP@CNXL particles prepared at 100 °C, 17 h, and 2% w/w for precursor to CNXL. Solid lines are drawn to guide the eye.

as shown in Figure 1. FTIR spectra of the actone-washed product showed the appearance of a new peak at about 1710 cm^{-1} (Supporting Information), attributed to the carbonyl stretch of aliphatic ketone and carboxylic acid formation due to oxidation of the cellulose surface,[51] which provides the driving force for the reduction of Pd(II) to Pd(0). The oxophilicity of Pd[52] then provides ample attractive interaction with the oxidized cellulose to remain attached to the surface and form PdNP@CNXL. The PdNPs were not removed during the acetone wash indicating sufficiently strong interactions. The CNXLs thus act as both the reducing agent and the support material, similar to our previous work on Ag and Pt in aqueous solutions.[35−37]

The mean diameter of synthesized PdNPs based on the XRD data (Figure 2(a)) increases with increasing pressure until 1000−1100 psi, at which point carbon dioxide changes from gas to supercritical, followed by a decrease in diameter at 2200 psi. Performing the reduction at 3500 psi resulted in the absence of any Pd peaks in the XRD spectrum, indicating no Pd reduction by the cellulosic surface. The relative height of the carbonyl stretch at 1710 cm^{-1} follows a similar trend to the PdNP mean diameter (Figure 2(b)). However, the lowest carbonyl content was determined for the largest particle size, with a minimum in the trend appearing around 1000−1100 psi, the gas supercritical phase transition point.

The Pd loading on CNXL also shows a dramatic effect at the phase transition between gas and supercritical CO_2 (Figure 3). The Pd content increased with increasing pressure until the critical pressure is reached, resulting in a dramatic reduction in Pd loading, which then stays roughly constant over the whole measured supercritical pressure range at about 25 wt % (no Pd loading was measured at 3500 psi confirming XRD results). The large dip in Pd loading at the critical transition may be due to surface effects where supercritical phase formation is seeded at the CNXL surface rather than in the CO_2 bulk. This would drastically reduce access to the surface and may even create convective movement away from the surface, thus lowering Pd reduction.

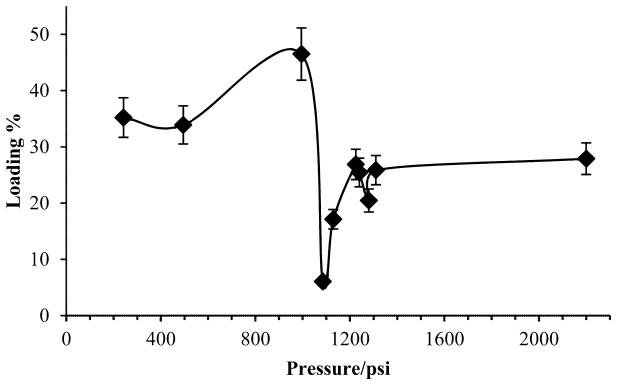

Figure 3. Effect of pressure on the loading percentage of synthesized PdNP@CNXLs prepared at 100 °C, 17 h, and 2% w/w for precursor to CNXL as obtained from TGA analysis.

It thus appears that Pd reduction at pressures well above the supercritical point behaves similar to Pd reduction at pressures well below the supercritical point. This indicates that Pd concentration is extremely important in determining PdNP loading, particle size for a given reaction time, and the extent of cellulose surface oxidation. As these findings are within expectations and the increased pressure would require unnecessary additional costs for commercial production, we decided not to add further samples in the 1400−2200 psi range.

XPS analysis of the samples shows the same behavior around the supercritical transition point. The Pd_{total}/C and Pd(0)/C ratios peak at the highest gaseous pressure and reduce upon breaching the critical pressure point of the gas supercritical phase transition (Figure 4). The amount of Pd(II) on the CNXLs does not appear to be strongly affected by the pressure, even though it shows a slight dip around the gas supercritical phase transition. It is found to be always significantly lower (less than 20%) than the amount of reduced Pd(0). The reason for the near-constant Pd(II) content may be that the Pd(II) in the nanoparticles appear at the interface with the CNXLs and form the bonds that keeps the PdNPs attached to the CNXLs. Indeed, they were not washed off, meaning that the interaction between PDNPs and CNXLs must be quite strong. It shows that most of the Pd supported on the surface of cellulose has indeed been reduced to Pd(0). The cellulose O/C ratio follows the same trend as the Pd_{total}/C and Pd(0)/C ratios. The theoretical O/C ratio for pure cellulose is 0.83, while the experimental ratio determined by XPS can be smaller due to carbonaceous species adsorbed onto the CNXL surface.[53] For the CNXL used in this work, we determined a ratio of 0.78. Upon reduction of Pd(II), this ratio goes through a small dip, rises toward the pure cellulose ratio, and then decreases again above the gas supercritical transition pressure (Figure 4(b)). The pure cellulose ratio is achieved where the carbonyl stretch vibration signal in FTIR reaches a maximum. The TGA showed the highest Pd loading, and XRD determined the largest Pd mean particle size.

The solubility of metal complexes with fluorinated ligands in CO_2 increases with increasing pressure.[54,55] This results in increased reduction of Pd(II) to Pd(0) with increasing CO_2 pressure below supercritical conditions, as evident by the increased Pd loading and higher PdNP mean size/diameter.

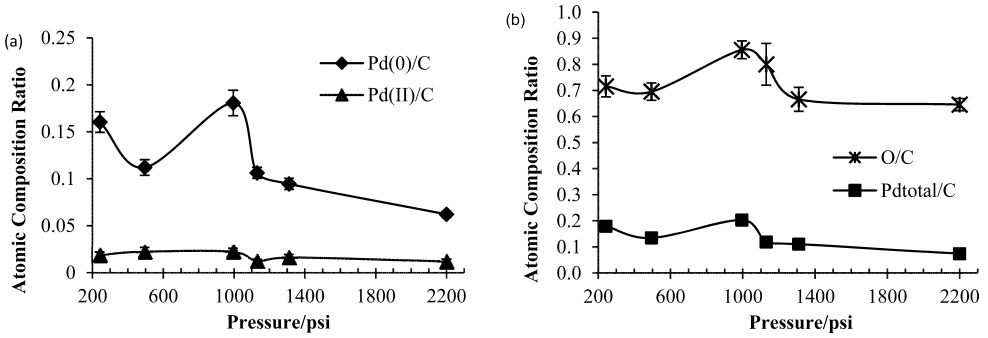

Figure 4. Effect of pressure on the atomic surface composition of the synthesized PdNP@CNXLs as prepared at 100 °C, 17 h, and 2% w/w for precursor to CNXL. Error bars denote 1 standard deviation (for Pd_{total}/C in (b), error bars are smaller than data points).

The concurrent oxidation of the CNXL surface occurs in the absence of oxygen, so it can be expected to first result in ketone/aldehyde formation through dehydrogenation as has been shown for other alcohols.[56] This will keep the O/C ratio constant but will result in the appearance of a C═O stretch signal in FTIR in the initial stages of Pd reduction. Further oxidation of the cellulose surface to drive Pd(II) reduction cannot occur by conversion of aldehydes to carboxylates using atmospheric oxygen due to oxygen-free reaction conditions. Under oxygen-free conditions, however, ethanol has been shown to decompose to CH_4, CO, H_2, and CO_2.[56] The increasing O/C ratio as the Pd around the gas supercritical phase transition indicates a depletion of oxygen relative to carbon. This happens at the same time as a decrease in relative intensity of the carbonyl stretch, indicating degradation of the cellulose surface through formation and release of CO_2 (thus decreasing C═O signal) as a result of Pd reduction. This degradation of cellulose is coupled with an increase in particle size and Pd loading. It appears that at a certain point, the top cellulose layer is so degraded that the pure underlying cellulose is exposed, giving a O/C ratio close to the ratio expected for pure cellulose (0.83), which then further oxidizes (increasing O/C ratio and increasing C═O stretch).

Furthermore, in the $scCO_2$ phase, the Pd(II)-to-Pd(0) increases with increasing pressure, indicating that Pd reduction becomes less favorable due to the gaseous byproducts that are required to be formed. The absence of reduction at very high pressures (3500 psi) results from known attractive interactions between CO_2 and hydroxyl and carbonyl groups. This may result in a barrier of CO_2 molecules, blocking or severely hindering access of Pd(II) to the surface hydroxyl groups where reduction has to occur.[57,58]

Effect of Reaction Time. The effect of the reaction time on the synthesized PdNPs supported on CNXL was studied in the range of 2−17 h, while pressure, temperature, and weight ratio of $(Pd(hfac)_2)$ to CNXL were fixed at 1300 psi, 100 °C, and 2% w/w, respectively (Figure 5). The mean size of PdNP@CNXL particles was found to increase with increasing reaction time up to 14 h (Figure 6). At 17 h, however, the mean diameter is shown to decrease. This suggests that the maximum diameter of supportable Pd nanoparticles on CNXLs is around 12−13 nm. This is twice the size of the CNXL cross section (cotton-derived CNXLs have a cross section of about 6.1 nm[59]).

The relative intensity of the carbonyl stretch concurrently increased for low reaction times and went through a slight dip as the reaction time further increased (Figure 6(a)). Compared with the Pd loading obtained from TGA, one notices that it follows a wavy curve as well but not in phase with the carbonyl

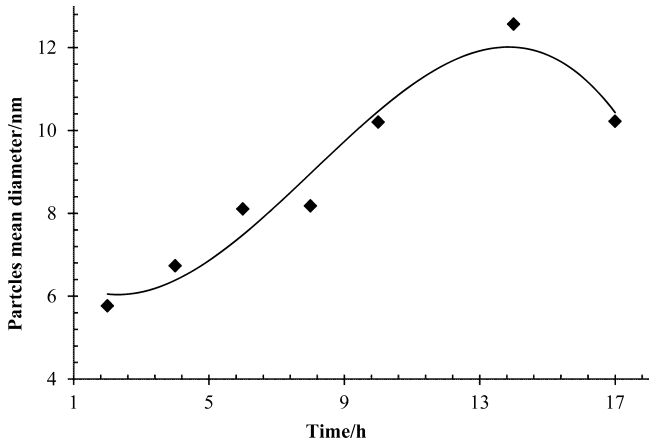

Figure 5. Effect of time reaction on the mean diameter (based on XRD experiments) of the synthesized PdNs supported on CNXL at 100 °C, 1300 psi, and 2% w/w for precursor to CNXL. The line is drawn to guide the eye.

stretch data, further suggesting that Pd is reduced by cellulose and part of the glucose units are consumed in the process as postulated before (through formation of ketones and aldehydes followed by CO_2 formation). It appears that initially the surface cellulose layer is oxidized, thereby increasing the measured carbonyl signal. Longer reaction times result in further oxidation and thus decomposition of the surface cellulose chains thereby reducing the carbonyl signal, followed by oxidation of the subsequent cellulose chains (increase in C═O vibration).

TGA determination of Pd loading on the PdNPs@CNXL composites shows a very surprising trend (Figure 6(b)). Whereas the maximum Pd loading is found for the largest particle mean diameter as could be expected, loading is found to go through a minimum around the same time where the carbonyl stretch signal starts to reduce in size. Because this occurs at the same time as a continuous increase in average particle size (Figure 5), this can only be the result of PdNP detachment from the CNXL surface as they become too big. We thus propose the following mechanism. Initially, Pd particles are seeded, and each grows at different speeds. As they reach a critical diameter of around 13 nm, they detach. The larger particles contain the largest relative amount of Pd, enabling a decrease in overall Pd content even when the average size increases with time. At around 8 h, with the average particle diameter around 8 nm (and Pd loading ∼15%), the decrease in loading is reversed as the difference in Pd content in detaching particles and remaining particles becomes

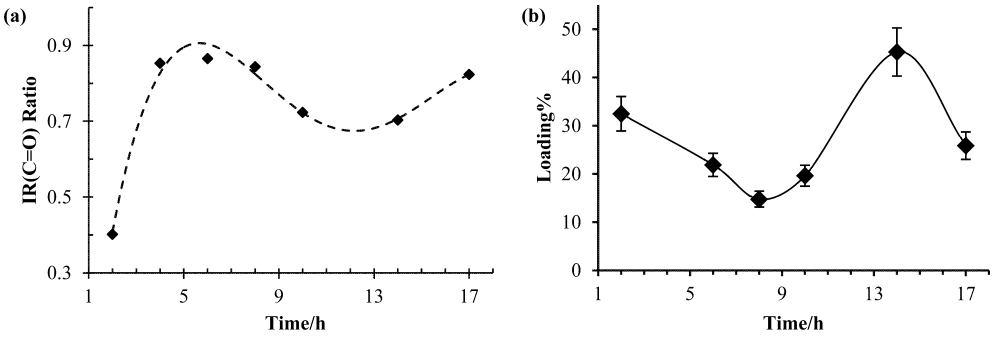

Figure 6. Effect of reaction time on (a) the relative intensity of the peaks 1710 cm^{-1} to 1630 cm^{-1} and (b) Pd loading for the synthesized PdNPs@CNXLs at 100 °C, 1300 psi, and 2% w/w for precursor to CNXL.

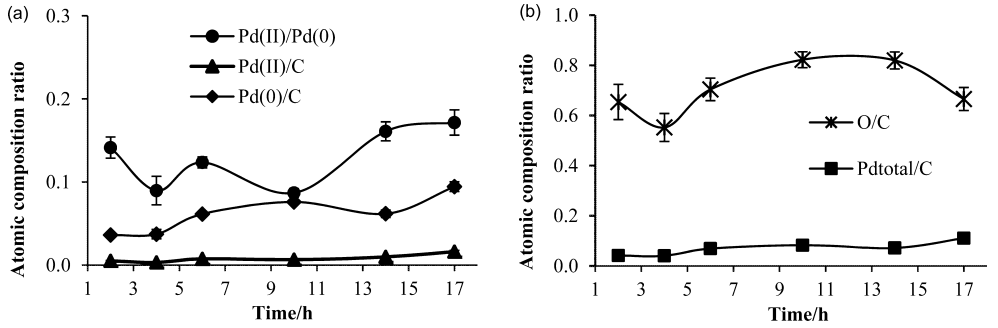

Figure 7. Effect of reaction time on the atomic surface composition of the synthesized PdNP@CNXLs at 100 °C, 1300 psi, and 2% w/w for precursor to CNXL. Error bars have the size of a standard deviation.

smaller. If none of the existing PdNPs formed at 8 h would detach, the Pd loading at 14 h (diameter 13 nm) would be approximately 65%, well above the maximum value of 45% in our samples, indicating that nanoparticle detachment does occur and that this is a viable hypothesis.

XPS analysis shows a similar trend for both the Pd(0) and Pd(II) to C ratio for the PdNPs as shown for the Pd content in the PdNP@CNXL materials (Figure 7). A higher ratio of Pd(0) to C is obtained for a lower carbonyl stretch content of the CNXL, further showing that more reduction of Pd(II) has occurred. The Pd(II)/C ratio follows a similar albeit less pronounced trend. This provides further evidence of the theory that subsequent layers of CNXL are being oxidized throughout the Pd reduction process. The O/C ratio follows the same trend as the TGA data, in line with the behavior shown for the Pd loading and O/C ratio with varying pressure (Figure 4).

Effect of Weight Ratio. The effect of the weight ratio of precursor ($Pd(hfac)_2$) to CNXL was studied in the range of 1−4% w/w (CNXL weight kept constant, $Pd(hfac)_2$ weight varied) while pressure, temperature, and reaction time were fixed at 1330 psi, 100 °C, and 10 h, respectively (Table 1). Surprisingly, the PdNP mean diameter and loading go through a maximum and minimum, respectively, at a 2% w/w precursor to CNXL ratio. The atomic O/C ratio remains rather constant between 0.85 and 0.81. The maximum in PdNP diameter occurs at roughly the same particle size as the maximum shown for increasing reaction times, indicating that 10−12 nm may be the upper limit for supported PdNP@CNXLs.

Table 1. Results of XRD, TGA, and XPS at Different Weight Ratios of Precursor to CNXL

weight ratio (% w/w)	PdNPs mean diameter (nm)	loading (wt %)	O/C
1	7	37.8	0.85
2	10	21.3	0.82
4	7	30.2	0.81

These combined results follow similar behavior as was shown for the constant ratio of precursor to CNXL with increasing reaction time. At lower weight ratios (1 and 2% w/w), increasing the weight ratio leads to larger PdNPs with lower overall Pd loading for a constant reaction time (same effect as shown for a constant ratio and increasing reaction time up until 10 h). Increasing the ratio further leads to an increase in Pd loading but also reduces the PdNP diameter as the larger particles detach. The slight decrease in O/C ratio is indicative of increased oxidation of the cellulose surface through CO_2 formation, in line with increased reduction of Pd(II) with increasing precursor loading.

PdNP@CNXL Visualization. The XRD diffractograms (Figure 1) show the retention of the CNXL crystalline structure for all the obtained PdNP@CNXL composites. However, electron microscopy was used to confirm the retention of the CNXLs' rodlike structure and to confirm the presence of PdNPs on the surface of the CNXLs (Figure 8). Samples were run after deposition of the nanoparticles from DMF dispersion directly, and some were stained with a 2 wt % aqueous uranyl acetate solution in order to more clearly show the CNXLs. In the unstained samples (Figure 8(A,B)), the PdNPs are clearly visible and are shown sitting on a substrate slightly darker than the carbon coating. Analysis of the nanowhisker diameters shows them to be in broad agreement with XRD measurements, while the crystal plane diffraction is shown in high magnification confirming the crystalline nature of the PdNPs (Supporting Information). Stained samples show the PdNP@CNXL composites to exist as aggregates of rodlike

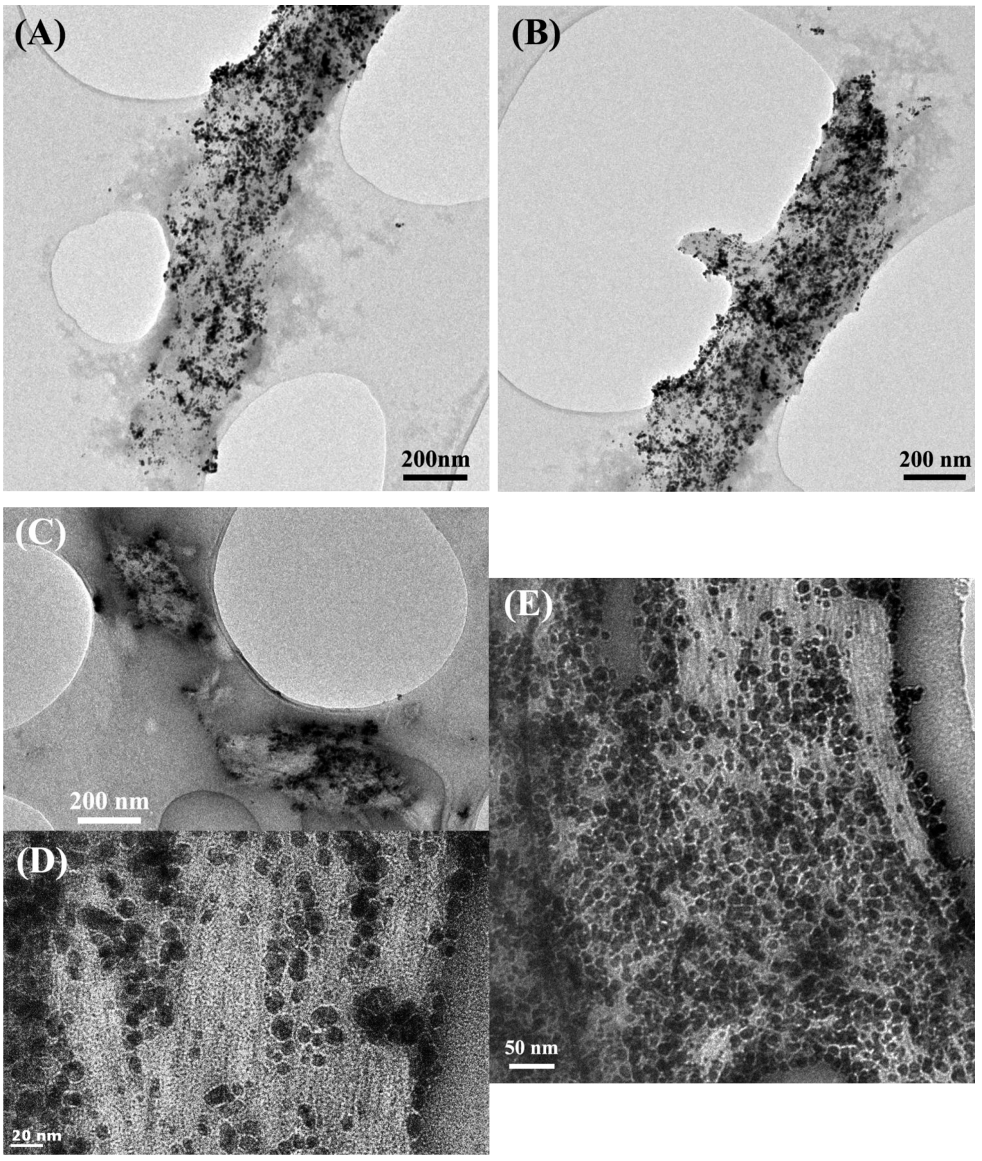

Figure 8. TEM micrographs of (A, B) unstained deposits of PdNP@CNXLs and (C–E) PdNP@CNXL deposites stained with uranyl acetate. Stained samples show the expected structure of CNXL aggregates.

structures on the surface of which the PdNPs can be found (Figure 89(C–E)). No individual nanowhiskers with PdNPs were found on the stained samples, but this could be due to the relatively high concentration of the dispersion used for sample preparation and drying conditions. The relative size of the PdNPs@CNXL is further in agreement with the size/diameter determined from XRD Scherrer fitting analysis.

Catalytic Activity. The synthesis of carbon–carbon bonds via palladium-catalyzed cross coupling methodology is extremely important for the synthesis of added-value organic molecules.[60] The utility of the method stems from the generality of the technique and functional group compatibility and the fact that it allows for the facile synthesis of complex molecules.[61] Despite the many advantages of this process, problems associated with catalyst separation, sensitivity to air/moisture, and toxicity of the frequently used phosphine ligands persist.[62] The use of solid supports[63−65] and nanoparticles[66] has been investigated to overcome some of these problems, although the often lengthy preparation times and difficulties in isolation of the catalysts can limit the overall utility of these approaches. In contrast, the PdNP@CNXL catalyst is easy to synthesize from a renewable feedstock without the need for an exogenous reducing agent. PdNP@CNXL displayed good catalytic activity in the Mizoroki–Heck reaction, i.e., the addition of an arylhalide to an alkene. For example, iodobenzene (**1**) underwent a smooth coupling with methyl acrylate to give methyl *trans*-cinnamate (**2**) in excellent yield under standard reaction conditions (Scheme 3), showing that

Scheme 3. PdNP@CNXL-Catalyzed Heck Reactions

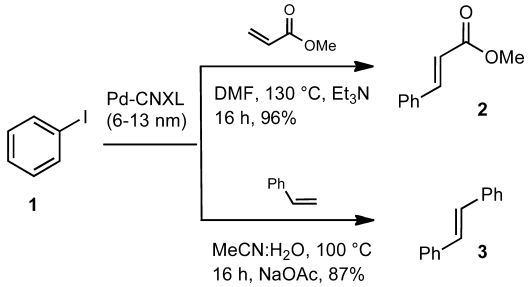

dx.doi.org/10.1021/sc500079q | ACS Sustainable Chem. Eng. 2014, 2, 1241−1250

Table 2. Comparison of Pd−Cellulose Catalysts for the Mizoroki−Heck Reaction

author	Pd−cellulose formation	catalyst size (nm)	cross-coupling conditions	product	yield (%)
Reddy[68]	$PdCl_2$, MC,[a] NH_2NH_2 MeOH, rt, 12 h	10−20	Et_3N, MeCN, 82 °C	**2**	98
			Et_3N, DMF, 120 °C	**3**	100
Cui[69]	$PdCl_2$, cellulose, EtOH, 60 °C, 72 h	N/A	Et_3N, H_2O, 90 °C	**3**	98
Moores[13]	$PdCl_2$, CNC,[b] HCl H_2O;	3.6 ± 0.8	K_2CO_3, H_2O/MeCN, 100 °C	**3**	75
	H_2 (4 bar), 2 h				
Tang[70]	$PdCl_2$, BC,[c] 140 °C, 5 h	40	Et_3N, DMF, 120 °C	**2**	94
	$NaBH_4$, 80 °C, 3 h		Et_3N, DMF, 100 °C	**3**	86
Li[71]	$PdCl_2$, DPPC,[d] EtOH reflux, 24 h	3−10	Et_3N, DMF, 110 °C	**3**	91
Shaabani72	$PdCl_2$, EDAC,[e] rt, 24 h	4.6−6.8	K_2CO_3, H_2O, 100 °C	**2**	98
	$NaBH_4$, rt, 5 h		K_2CO_3, H_2O, 100 °C	**3**	99

[a]Microcrystalline cellulose. [b]Colloidal cellulose nanocrystallites. [c]Bacteria cellulose. [d]Diphenylphosphinite cellulose (∼5 d preparation). [e]Ethylenediamine-functionalized cellulose (∼48 h preparation).

supporting the PdNPs on cellulose does not affect its activity.[67] Additionally, the unactivated alkene styrene reacted under aqueous Mizoroki−Heck conditions to afford the desired addition adduct **3** in good yield. Direct comparison of this approach to other palladium−cellulose catalysts systems developed by Reddy,[68] Cui,[69] Moores,[13] Tang,[70] Li,[71] and Shaabani[72] is difficult due to the stark differences in the preparation of the catalysts and coupling reaction conditions (Table 2). However, our results fit squarely within the range of yields and nanoparticle sizes previously reported but without the need for an organic solvent, exogenous reducing agent, or extended reaction time to form and isolate the catalyst.

CONCLUSION

PdNPs supported on CNXL were synthesized using subcritical and supercritical CO_2 in one step. Relying on the FTIR and XRD results, CNXL could play as both a reduction agent and biomass supporter in this work. The pressure, reaction time, and weight ratio of precursor Pd(hfac) could control the particle mean diameter and loading percent of Pd@CNXL. The maximum mean diameter of PdNPs was about 13 nm, where pressure, temperature, reaction time, and weight ratio of the precursor to CNXL were 1300 psi, 100 °C, 10 h, and 2% w/w, respectively. Also, under these conditions, the loading percent of PdNPs@CNXL was at the maximum value, 45% w/w. TGA results confirmed that PdNPs supported on cellulose increased the combustion temperature of the treated CNXL comparing to untreated CNXL. Finally, these nanoparticles were shown to be catalytically active in palladium-mediated cross-coupling reactions of arylhalides and alkenes.

ASSOCIATED CONTENT

Supporting Information

Representative FTIR and XPS spectra as well as a high resolution PdNP TEM micrograph. This material is available free of charge via the Internet at http://pubs.acs.org.

AUTHOR INFORMATION

Corresponding Author

*E-mail: Wim.Thielemans@kuleuven.be.

Present Addresses

[⊥]W. Thielemans: KU Leuven, Kortrijk Campus, Etienne Sabbelaan 53, 8500 Kortrijk, Belgium.

[#]M. Rezayat: Chemical Physical Laboratory Center, Arfa Iron and Steel Co., Yzad 19679-17183, Islamic Republic of Iran.

Notes

The authors declare no competing financial interest.

ACKNOWLEDGMENTS

W. Thielemans and D. A. Walsh thank the Engineering and Physical Sciences Research Council (EPSRC) for financial support under the DICE project (EP/D501229/1), as well as Emily Smith at the University of Nottingham XPS service. R. K. Blundell and J. E. Camp also thank the UKRC's work placement bursary scheme 2010−2011 for financial support of R.K.B.'s summer studentship.

REFERENCES

(1) Burda, C.; Chen, X.; Narayanan, R.; El-Sayed, M. A. Chemistry and properties of nanocrystals of different shapes. *Chem. Rev.* **2005**, *105*, 1025−1102.

(2) Reetz, M. T.; Breinbauer, R.; Wanniger, K. Suzuki and Heck reactions catalyzed by preformed palladium clusters and palladium/nickel bimetallic clusters. *Tetrahedron Lett.* **1996**, *37*, 4499−4502.

(3) Beller, M.; Fischer, H.; Kühlein, K.; Reisinger, C.-P.; Hermann, W. A. First palladium-catalyzed Heck reactions with efficient colloidal catalyst systems. *J. Organomet. Chem.* **1996**, *520*, 257−259.

(4) Kogan, V.; Aizenshtat, Z.; Popovitz-Biro, R.; Neumann, R. Carbon−carbon and carbon−nitrogen coupling reactions catalyzed by palladium nanoparticles derived from a palladium substituted Keggin-type polyoxometalate. *Org. Lett.* **2002**, *4*, 3529−3532.

(5) Scholten, J. D.; Leal, B. C.; Dupont, J. Transition metal nanoparticle catalysis in ionic liquids. *ACS Catal.* **2012**, *2*, 184−200.

(6) Yan, N.; Xiao, C.; Kou, Y. Transition metal nanoparticle catalysis in green solvents. *Coord. Chem. Rev.* **2010**, *254*, 1179−1218.

(7) Torborg, C.; Beller, M. Recent applications of palladium-catalyzed coupling reactions in the pharmaceutical, agrochemical, and fine chemical industries. *Adv. Synth. Catal.* **2009**, *351*, 3027−3043.

(8) Blaser, H.-U; Indolese, A.; Schnyder, A.; Steiner, H.; Studer, M. Supported palladium catalysts for fine chemicals synthesis. *J. Mol. Catal. A: Chem.* **2001**, *173*, 3−18.

(9) Molnar, A.; Papp, A. The use of polysaccharides and derivatives in palladium-catalyzed coupling reactions. *Catal. Sci. Technol.* **2014**, *4*, 295−310.

(10) Wu, H.; Zhuo, L.; He, Q.; Liao, X.; Shi, B. Heterogeneous hydrogenation of nitrobenzenes over recyclable Pd(0) nanoparticle catalysts stabilized by polyphenol-grafted collagen fibers. *Appl. Catal., A* **2009**, *366*, 44−56.

(11) MacQuarrie, S.; Horton, J. H.; Barnes, J.; McEleney, K.; Loock, H.-P.; Crudden, C. M. Visual observation of redistribution and dissolution of palladium during the Suzuki−Miyaura reaction. *Angew. Chem., Int. Ed.* **2008**, *47*, 3279−3282.

(12) Feng, J.; Yang, C.; Zhang, D.; Wang, J.; Fu, H.; Chen, H.; Li, X. Catalytic transfer hydrogenolysis of α-methylbenzyl alcohol using palladium catalysts and formic acid. *Appl. Catal., A* **2009**, *354*, 38−43.

(13) Cirtiu, C. M.; Dunlop-Brière, A. F.; Moores, A. Cellulose nanocrystallites as an efficient support for nanoparticles of palladium: application for catalytic hydrogenation and Heck coupling under mild conditions. *Green Chem.* **2011**, *13*, 288−291.
(14) Søbjerg, L. S.; Gauthier, D.; Lindhardt, A. T.; Bunge, M.; Finster, K.; Meyer, R. L.; Skrydstrup, T. Bio-supported palladium nanoparticles as a catalyst for Suzuki−Miyaura and Mizoroki−Heck reactions. *Green Chem.* **2009**, *11*, 2041−2046.
(15) Xu, L.; Wu, X.-C.; Zhu, J.-J. Green preparation and catalytic application of Pd nanoparticles. *Nanotechnology* **2008**, *19*, 305603.
(16) Mukherjee, D. Potential application of palladium nanoparticles as selective recyclable hydrogenation catalysts. *J. Nanopart. Res.* **2008**, *10*, 429−436.
(17) Liu, Q.; Bauer, J. C.; Schaak, R. E.; Lunsford, J. H. Supported palladium nanoparticles: An efficient catalyst for the direct formation of H_2O_2 from H_2 and O_2. *Angew. Chem.* **2008**, *120*, 6317−6320.
(18) Morales-Acosta, D.; Rodriguez G., H.; Godinez, L. A.; Arriaga, L. G. Performance increase of microfluidic formic acid fuel cell using Pd/MWCNTs as catalyst. *J. Power Sources* **2010**, *195*, 1862−1865.
(19) Thiagarajan, S.; Yange, R.-F.; Chen, S.-M. Palladium nanoparticles modified electrode for the selective detection of catecholamine neurotransmitters in presence of ascorbic acid. *Bioelectrochemistry* **2009**, *75*, 163−169.
(20) Nadagouda, M. N.; Polshettiwar, V.; Varma, R. S. Self-assembly of palladium nanoparticles: synthesis of nanobelts, nanoplates and nanotrees using vitamin B1, and their application in carbon−carbon coupling reactions. *J. Mater. Chem.* **2009**, *19*, 2026−2031.
(21) Raveendran, P.; Fu, J.; Wallen, S. L. Completely "green" synthesis and stabilization of metal nanoparticles. *J. Am. Chem. Soc.* **2003**, *125*, 13940−13941.
(22) Murphy, C. J. Sustainability as an emerging design criterion in nanoparticle synthesis and applications. *J. Mater. Chem.* **2008**, *18*, 2173−2176.
(23) Raveendran, P.; Fu, J.; Wallen, S. L. A simple and "green" method for the synthesis of Au, Ag, and Au−Ag alloy nanoparticles. *Green Chem.* **2006**, *8*, 34−38.
(24) Camp, J. E.; Dunsford, J. J.; Cannons, E. P.; Restorick, W. J.; Gadzhieva, A.; Fay, M. W.; Smith, R. J. Glucose-derived palladium(0) nanoparticles as in situ-formed catalysts for Suzuki−Miyaura cross-coupling reactions in isopropanol. *ACS Sustainable Chem. Eng.* **2014**, *2*, 500−505.
(25) Cai, J.; Kimura, S.; Wada, M.; Kuga, S. Nanoporous cellulose as metal nanoparticles support. *Biomacromolecules* **2009**, *10*, 87−94.
(26) Liu, J.; He, F.; Durham, E.; Zhao, D.; Roberts, C. B. Polysugar-stabilized pd nanoparticles exhibiting high catalytic activities for hydrodechlorination of environmentally deleterious trichloroethylene. *Langmuir* **2008**, *24*, 328−336.
(27) Shin, Y.; Bae, I.-T.; Arey, B. W.; Exarhos, G. J. Simple preparation and stabilization of nickel nanocrystals on cellulose nanocrystal. *Mater. Lett.* **2007**, *61*, 3215−3217.
(28) Evans, B. R.; O'Neill, H. M.; Malyvanh, V. P.; Lee, I.; Woodward, J. Palladium-bacterial cellulose membranes for fuel cells. *Biosens. Bioelectron.* **2003**, *18*, 917−923.
(29) Shin, Y.; Bae, I.-T.; Arey, B. W.; Exarhos, G. J. Facile stabilization of gold-silver alloy nanoparticles on cellulose nanocrystal. *J. Phys. Chem. C* **2008**, *112*, 4844−4848.
(30) Shin, Y.; Blackwood, J. M.; Bae, I.-T.; Arey, B. W.; Exarhos, G. J. Synthesis and stabilization of selenium nanoparticles on cellulose nanocrystal. *Mater. Lett.* **2007**, *61*, 4297−4300.
(31) Wu, X.; Lu, C.; Zhou, Z.; Yuan, G.; Xiong, R.; Zhang, X. Green synthesis and formation mechanism of cellulose nanocrystal-supported gold nanoparticles with enhanced catalytic performance. *Environ. Sci.: Nano* **2014**, *1*, 71−79.
(32) Jamwal, N.; Sodhi, R. K.; Gupta, P.; Paul, S. Nano Pd(0) supported on cellulose: A highly efficient and recyclable heterogeneous catalyst for the Suzuki coupling and aerobic oxidation of benzyl alcohols under liquid phase catalysis. *Int. J. Biol. Macromol.* **2011**, *49*, 930−935.
(33) Zhou, P.; Wang, H.; Yang, J.; Tang, J.; Sun, D.; Tang, W. Bio-supported palladium nanoparticles as a phosphine-free catalyst for the Suzuki reaction in water. *RSC Adv.* **2012**, *2*, 1759−1761.
(34) Wu, X.; Lu, C.; Zhang, W.; Yuan, G.; Xiong, R.; Zhang, X. A novel reagentless approach for synthesizing cellulose nanocrystal-supported palladium nanoparticles with enhanced catalytic performance. *J. Mater. Chem. A* **2013**, *1*, 8645−8652.
(35) Benaissi, K.; Johnson, L.; Walsh, D. A.; Thielemans, W. Synthesis of platinum nanoparticles using cellulosic reducing agents. *Green Chem.* **2010**, *12*, 220−222.
(36) Johnson, L.; Thielemans, W.; Walsh, D. A. Nanocomposite oxygen reduction electrocatalysts formed using bioderived reducing agents. *J. Mater. Chem.* **2010**, *20*, 1737−1743.
(37) Johnson, L.; Thielemans, W.; Walsh, D. A. Synthesis of carbon-supported Pt nanoparticle electrocatalysts using nanocrystalline cellulose as reducing agent. *Green Chem.* **2011**, *13*, 1686−1693.
(38) Koga, H.; Tokunaga, E.; Hidaka, M.; Umemura, Y.; Saito, T.; Isogai, A.; Kitaoka, T. Topochemical synthesis and catalysis of metal nanoparticles exposed on crystalline cellulose nanofibers. *Chem. Commun.* **2010**, *46*, 8567−8569.
(39) Byrappa, K.; Ohara, S.; Adschiri, T. Nanoparticles synthesis using supercritical fluid technology - towards biomedical applications. *Adv. Drug Delivery Rev.* **2008**, *60*, 299−327.
(40) Colin, R. Renewables and green chemistry. *Green. Chem.* **2005**, *7*, 57.
(41) Cansell, F.; Aymonier, C.; Loppinet-Serani, A. Review on materials science and supercritical fluids. *Curr. Opin. Solid State Mater. Sci.* **2003**, *7*, 331−340.
(42) Oakes, R. S.; Clifford, A. A.; Rayner, C. M. The use of supercritical fluids in synthetic organic chemistry. *J. Chem. Soc., Perkin Trans. 1* **2001**, *1*, 917−941.
(43) Leitner, W. Supercritical carbon dioxide as a green reaction medium for catalysis. *Acc. Chem. Res.* **2002**, *35*, 746−756.
(44) Rollins, H. W. In *Dekker Encyclopedia of Nanoscience and Nanotechnology*, 2nd ed.; Cristian, I., Contescu, C. I., Putyera, K. CRC Press: Boca Raton, FL, 2009; p 2072.
(45) Kelly, M. J.; Kim, J.; Roberts, G. W.; Lamb, H. H. Characterization of Pd/γ-Al_2O_3 catalysts prepared using [$Pd(hfac)_2$] in liquid CO_2. *Top. Catal.* **2008**, *49*, 178−186.
(46) Heath, L.; Thielemans, W. Cellulose nanowhisker aerogels. *Green Chem.* **2010**, *12*, 1448−1453.
(47) Vinkevicius, J.; Jankauskas, E.; Cerskiene, I.; Jasulaitiene, V.; Vaskelis, A. Interaction of cobalt sulphide coatings with Pd(II) ions: Cyclic voltammetry and XPS study. *Chemija* **2004**, *15*, 11−16.
(48) Zhang, Z.; Zha, Z.; Gan, C.; Pan, C.; Zhou, Y.; Wang, Z.; Zhou, M.-M. Catalysis and regioselectivity of the aqueous Heck reaction by Pd(0) nanoparticles under ultrasonic irradiation. *J. Org. Chem.* **2006**, *71*, 4339−4342.
(49) Dong, D.-J.; Li, H.-H.; Tian, S.-K. A highly tunable stereoselective olefination of semistabilized triphenylphosphonium ylides with *N*-sulfonyl imines. *J. Am. Chem. Soc.* **2010**, *132*, 5018−5020.
(50) Nishiyama, Y.; P. Langan, P.; Chanzy, H. Crystal structure and hydrogen-bonding system in cellulose Iβ from synchrotron X-ray and neutron fiber diffraction. *J. Am. Chem. Soc.* **2002**, *124*, 9074−9082.
(51) Pandey, K. K. A study of chemical structure of soft and hardwood and wood polymers by FTIR spectroscopy. *J. Appl. Polym. Sci.* **1999**, *71*, 1969−1975.
(52) Arenz, M.; Stamenkovic, V.; Ross, P. N.; Markovic, N. M. Preferential oxidation of carbon monoxide adsorbed on Pd submonolayer films deposited on Pt(1 0 0). *Electrochem. Commun.* **2003**, *5*, 809−813.
(53) M. Labet, M.; Thielemans, W. Improving the reproducibility of chemical reactions on the surface of cellulose nanocrystals: ROP of ε-caprolactone as a case study. *Cellulose* **2011**, *18*, 607−617.
(54) Smart, G.; Carleson, T.; Kast, T.; Clifford, A. A.; Burford, M. D.; Wai, C. M. Solubility of chelating agents and metal-containing compounds in supercritical fluid carbon dioxide. *Talanta* **1997**, *44*, 137−150.

(55) Hasell, T.; Wood, C. D.; Clowes, R.; Jones, J. T. A.; Khimyak, Y. Z.; Adams, D. J.; Cooper, A. I. Palladium nanoparticle incorporation in conjugated microporous polymers by supercritical fluid processing. *Chem. Mater.* **2010**, *22*, 557−564.
(56) Hohn, K. L.; Lin, Y. C. Catalytic partial oxidation of methanol and ethanol for hydrogen generation. *ChemSusChem* **2009**, *2*, 927−940.
(57) Raveendran, P.; Wallen, S. L. Cooperative C−H···O hydrogen bonding in CO_2−Lewis base complexes: Implications for solvation in supercritical CO_2. *J. Am. Chem. Soc.* **2002**, *124*, 12590−12599.
(58) Blatchford, M. A.; Raveendran, P.; Wallen, S. L. Raman spectroscopic evidence for cooperative C−H···O interactions in the acetaldehyde−CO_2 complex. *J. Am. Chem. Soc.* **2002**, *124*, 14818−14819.
(59) Eyley, S.; Shariki, S.; Dale, S. E. C.; Bending, S.; Marken, F.; Thielemans, W. Ferrocene-decorated nanocrystalline cellulose with charge carrier mobility. *Langmuir* **2012**, *28*, 6514−6519.
(60) Yin, L.; Liebscher, J. Carbon−carbon coupling reactions catalyzed by heterogeneous palladium catalysts. *Chem. Rev.* **2007**, *107*, 133−173.
(61) Tsuji, J. *Palladium Reagents and Catalysis; Innovations in Organic Synthesis*; Wiley: Chichester, U.K., 1996.
(62) Polshettiwar, V.; Nadagouda, M. N.; Varma, R. S. The synthesis and applications of a micro-pine-structured nanocatalyst. *Chem. Commun.* **2008**, 6318−6320.
(63) Clark, J. H.; Macquarrie, D. J.; Mubofu, E. B. Preparation of a novel silica-supported palladium catalyst and its use in the Heck reaction. *Green Chem.* **2000**, *2*, 53−55.
(64) Morisaki, Y.; Ishida, T.; Chujo, Y. Synthesis and characterization of dithia[3.3](2,6)pyridinophane-containing polymers: application to the palladium-catalyzed Heck reaction. *Org. Lett.* **2006**, *8*, 1029−1032.
(65) Bernini, R.; Cacchi, S.; Fabrizi, G.; Forte, G.; Petrucci, F.; Prastaro, A.; Niembro, S.; Shafir, A.; Vallribera, A. Perfluoro-tagged, phosphine-free palladium nanoparticles supported on silica gel: Application to alkynylation of aryl halides, Suzuki−Miyaura cross-coupling, and Heck reactions under aerobic conditions. *Green Chem.* **2010**, *12*, 150−158.
(66) Hagiwara, H.; Sugawara, Y.; Isobe, K.; Hoshi, T.; Suzuki, T. Immobilization of Pd(OAc)(2) in ionic liquid on silica: Application to sustainable Mizoroki−Heck reaction. *Org. Lett.* **2004**, *6*, 2325−2328.
(67) Rocaboy, C.; Gladysz, J. A. Highly active thermomorphic fluorous palladacycle catalyst precursors for the Heck reaction; Evidence for a palladium nanoparticle pathway. *Org. Lett.* **2002**, *4*, 1993−1996.
(68) Reddy, K. R.; Kumar, N. S.; Reddy, P. S.; Sreedhar, B.; Kantam, M. L. Cellulose supported palladium(0) catalyst for Heck and Sonogashira coupling reactions. *J. Mol. Cat. A: Chem.* **2006**, *252*, 12−16.
(69) Xu, Y.; Zhang, L.; Cui, Y. Catalytic performance of cellulose supported palladium complex for Heck reaction in water. *J. Appl. Polym. Sci.* **2008**, *110*, 2996−3006.
(70) Zhou, P.; Wang, H.; Yang, J.; Tang, J.; Sun, D.; Tang, W. Bacteria cellulose nanofibers supported palladium(0) nanocomposite and its catalysis evaluation in Heck reaction. *Ind. Eng. Chem. Res.* **2012**, *51*, 5743−5748.
(71) Du, Q.; Li, Y. Application of an air-and-moisture-stable diphenylphosphinite cellulose-supported nanopalladium catalyst for a Heck reaction. *Res. Chem. Intermed.* **2012**, *38*, 1807−1817.
(72) Keshipour, S.; Shojaei, S.; Shaabani, A. Palladium nano-particles supported on ethylenediaminefunctionalized cellulose as a novel and efficient catalyst for the Heck and Sonogashira couplings in water. *Cellulose* **2013**, *20*, 973−980.